Thermochimica Acta, 203 (1992) 321–337
Elsevier Science Publishers B.V., Amsterdam

Problems of $YBa_2Cu_3O_x$ formation and decomposition kinetics and mechanism

Jaroslav Šesták [a] and Nobuyoshi Koga [b]

[a] *Department of Chemistry, Institute of Physics, Czech Academy of Sciences, Na Slovance 2, CS-18040 Prague 8 (Czech and Slovak Federal Rep.)*
[b] *Chemistry Laboratory, Faculty of School Education, Hiroshima University, Shinonome, Minami-ku, Hiroshima 734 (Japan)*

(Received 3 September 1991; in revised form 18 November 1991)

Abstract

The kinetics and mechanism of $YBa_2Cu_3O_x$ formation is reconsidered on the basis of literature data and our own data which have shown that their detailed solution from TA measurements alone is not feasible. Curves indicating morphological and chemical reactivity aspects are presented, diffusion and possibly two-dimensional nucleation being largely responsible for HTSC formation. The oxygen intake is also controlled by diffusion, and can strongly affect the high-temperature superconducting properties of the grain surface layer. The formation of intermediate superstructures is particularily noteworthy.

INTRODUCTION

Since the discovery of high T_c superconductors (HTSC), the analysis of their formation kinetics has become an important tool in the better understanding of the properties of the final products. The reactivity of the feed material was first investigated by means of DTA and TG [1–4] including the oxidation and reduction processes of the major superconducting compound [5–7] $YBa_2Cu_3O_x$ (abbreviated as 123) as well as its DTA characteristics [5,8,9]. Early kinetic analysis was applied to the final stage of thermal decomposition taking place above 750°C [1] with activation energy $E = 263$ kJ mol^{-1}. It was assumed [1] that a single reaction is responsible for the final decomposition of the coprecipitated oxalate precursor. Kinetic analysis of TG data for the final perovskite formation was also carried out, giving on activation energy of 282 kJ mol^{-1}, demonstrating again that the

Correspondence to: J. Šesták, Department of Chemistry, Institute of Physics, Czech Academy of Sciences, Na Slovance 2, CS-18040 Prague 8, Czechoslovakia.
Dedicated to Professor Joseph H. Flynn in honour of his 70th birthday.

0040-6031/92/$05.00 © 1992 – Elsevier Science Publishers B.V. All rights reserved

single process involved can be fitted by a phase-boundary-controlled reaction for contracting interfaces [1]. Le van Huan et al. [10] followed weight changes of the 123 phase formation taking place via intermediate phases with oxygen, CO_2 and feed oxides, the CO_2 being liberated not directly from the initial carbonates but from the intermediate phases which contain the incorporated $BaCO_3$. The mass transfer was found to be limited by the diffusion process (parabolic law) and proceeded at higher temperatures with increased activation energies (about 230 kJ mol^{-1}). Data for the perovskite formation have also been reported for a diffusion-controlled mechanism with $E = 269$ kJ mol^{-1} [1], most of these results being reviewed by Ozawa [11].

A detailed study was carried out by Gadalla and Hegg [12] who suggested that the formation of 123 compound involves three consecutive steps, including the reactions

$$BaCO_3 + CuO \rightarrow BaCuO_2 + CO_2 \quad (1)$$

$$Y_2O_3 + BaCuO_2 \rightarrow Y_2BaCuO_5 \quad (2)$$

$$Y_2BaCuO_5 + 3BaCuO_2 + 2CuO \rightarrow 2YBa_2Cu_3O_{6.5-x} + xO_2 \quad (3)$$

Wu and co-workers [13,14] showed that if $BaCuO_2$ is used as the Ba source instead of $BaCO_3$, the last two reaction steps become essential. It was noted that the reactant oxide in the last reaction was often detected as the major impurity phase in many incompletely reacted 123 powders. Furthermore, the previous studies [13,14] indicated that single-phase 123 powder could be obtained in a short time by synthesis via the last reaction. Gadalla and Hegg [12] were the only group who reported the kinetic parameters for each of the reaction steps listed above. From DTG, they calculated the activation energy for the third reaction which took place in series, following the other two earlier reaction steps. Their data were best fitted by three-dimensional diffusion, with E 419 kJ mol^{-1}. Wu et al. [15] demonstrated that the reaction mechanism scheme by detailed geometrical consideration of the steps involved in the solid-state reaction (3), is best fitted by the unreacted-core shrinking model (Ginstling–Brounshtein equation, D_3). The diffusion of Ba^{2+} is the limiting process, the pre-exponential factor changing with the reactant particle size. The activation energy, however, reached a value of 2277 kJ mol^{-1}, much larger than that reported in ref. 12, although the same experimental technique and evaluation was used in both works. This indicates the complexity of the reactions involved, each possibly being affected by other prior reactions and by the state of the feed precursor material. However, the assumingly Ba^{2+}-diffusion-controlled process studied above 900°C in ref. 15 can be compared with that of volume cation self-diffusion measured during sintering by dilatation [16] and creep [17], which give activation energies of, respectively, 1150 and 970 kJ.

REACTIVITY OF FEED MIXTURES AND THE SAMPLE MORPHOLOGY

The complexity of the reactions necessary to form the 123 product is apparent from the complex pattern of the DTA curves measured for the different starting mixtures and repeat runs, see Fig. 1. In general, the $BaCO_3 + CuO$ reaction is fast at first until $BaCuO_2$ envelopes the unreacted core, slowing down the escape of CO_2 by diffusion; while the $BaO + CuO$ reaction is more steadily fast. The $Y_2O_3 + 2CuO$ reaction is also fast at first but then slows down because of the decrease in the amount of feeding reactants. $BaCuO_2$ and $Y_2Cu_2O_5$ react very fast but their existence is usually limited up to a temperature of 950°C, while Y_2BaCuO_5 (211) starts to appear from 930°C, reaching its maximum at about 960°C, almost identical to 123. The decomposition of $BaCO_3$ occurs as high as 1200°C, but its solid-state reactivity increases above its transition at 813°C,

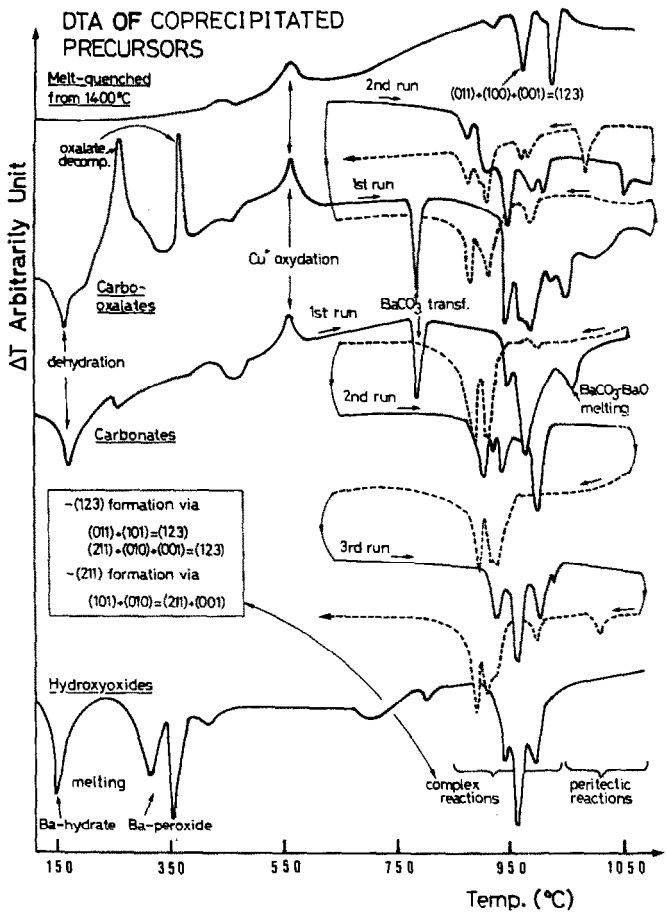

Fig. 1. DTA curves obtained at 5 K min^{-1} in flowing O_2 atmosphere, Pt cells with 200 mg charge using a Netzsch apparatus (the broken lines correspond to cooling).

being essentially accelerated by the formation of an intermediate compound $BaCO_3 \cdot BaO$ [2] which can melt as low as 1000°C. Peroxides and hydrates of BaO can increase the reactivity by low-temperature melting. It is worth noting that with increasing temperature the stability of Cu-based oxygen-poor solid phases can increase while that of oxygen-rich melt can decrease which may result in the strange effect of solidification on heating and, the reverse, in melting upon cooling. In addition the concave meniscus in small pores can enable liquation at a T_{melt} below that of bulk material (Bi_2O_3, AgO or PbO are common flux components that can accelerate this capillarity effect). The usually Cu-rich melts thus formed can enhance not only the mixture reactivity but also the surface glass-formation which consequently can close the pore network necessary to ensure free oxygen intake. This is often caused by segregation of a second (impurity) phase on the convex interfaces of very small particles which is a natural consequence of thermodynamics (Gibbs adsorption isotherm). The cation interface enrichment usually becomes effective for grain sizes as low as about 1 μm; the same size being found to behave as a mean superconducting domain (quasi-particle) [18], even for larger grains otherwise observed morphologically.

It became evident from the experiments that the composition and charge state of the very thin layers separating the superconducting particles are responsible for the transport properties determined. The supercurrent is maintained either by a small number of good superconducting contacts interconnecting the grains and/or by a small number of carriers tunnelling through the insulating barriers. Simultaneous measurements of negligible changes in oxygen content with respect to electrical resistivity [18] showed a correlation between the changes in the residual electrical resistivity and the weakening of the superconducting coupling between the grains. The onset of critical temperatures (where the superconductivity is first nucleated) was consequently found to be independent of the current density and weakly dependent on the magnetic field, whereas below the inflection point of T_c transition, the electrical resistivity and the superconducting percolation become strongly current and field dependent as a result of the formation of weak links owing to a very small oxygen interface depletion which modifies the tunneling probability among the quasi-particles. The thickness of such an insulating barrier is assumed to be in the order of 10^{-2}–10^{-3} μm [18]. Moreover, the local cation and anion contents can also be affected by the local stress state. In particular, a high elastic tension is expected in all polycrystalline orthorhombic aggregates, because the *c*-axis concentration from the formation temperature is about three times that of the *a*- and *b*-axis concentration. Stress minimizing is preferably achieved by the removal of oxygen from the stress sites, thus reducing there the lattice parameter but also locally degrading the superconducting state, once again producing weak links.

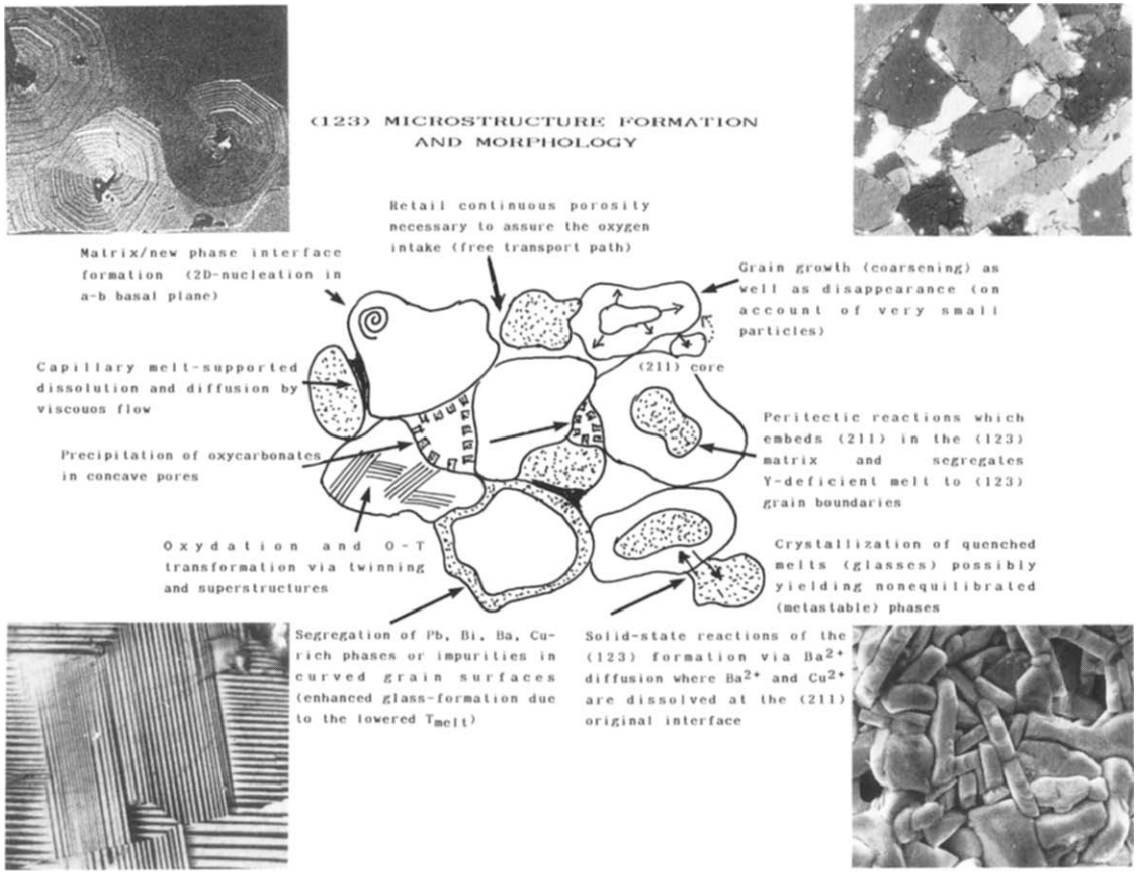

Fig. 2. Morphology schema (photographs provided by courtesy of Dr. P. Diko of the Institute of Experimental Physics, Kosice). Shaded area represents non-superconducting phases.

Illustrated examples include the microstructural observation of $YBa_{2-y}Pb_yCu_3O_x$ ceramics by Diko et al. [19]. Improved sintering due to PbO addition is caused by formation of the lead-rich liquid phase, whereas the lead itself is not dissolved in the entire 123 phase. Underneath a PbO-rich layer microns thick, another layer is formed exhibiting high porosity due to decreased sinterability. The PbO-rich surface envelope then controls the oxygen diffusion into the core and can have a secondary influence on the crystal growth of the 123 phase, the size of the grains being reduced by the rising PbO content [19]. However, the readily dissolved impurities in the bulk $YBa_2(Cu_{1-y}Me_y)_3O_x$ may again induce a pronounced oxygen redistribution, causing domain formation due to the uptake of excess oxygen (about one additional O per Me) which often leads to a fall in the orthorhombicity resulting from the equalization of the *a*- and *b*-axes. For example, it occurs for $y < 0.03$ if Me = Al, Co, Fe or Mn, which corresponds to an impurity concentration in the Cu(1) plane of up to 10% (because at least 75% of these Me impurities seem to prefer to occupy the Cu (1) sites). Furthermore, we cannot exclude the possible formation of as yet unknown metastable phases with varying cation ratios Y:Ba:Cu (calculated hypothetically in ref. 20), formed as a consequence of local thermodynamic instabilities, again probably located at energetically exposed areas such as curved interfaces and stress sites.

All these considerations imply that particle morphology is important for the preparation of high J_c HTSC. It is generally valid that with longer calcination times, larger particles with a broader size distribution are produced and a lower density of the sintered pellets is generated. Possible steps involved in the microstructure formation are illustrated in Fig. 2 which shows some of the problems limiting the J_c values, not including any additional effects created by mechanical disconnections (cracks), stacking faults, insulating layers, tetragonal strips, concentration gradients. The effect of non-equilibrated melts (formed during fast heating of not completely reacted feed mixtures) and associated temperature gradients creating the non-porous layers which then surround reacting grains, stopping the free passage of CO_2 [21], is worth noting. The presence of residual carbonates (or even carbon as the reduction product) in the grain interfaces often plays a major role in determining the J_c values [22]. However, such phase boundaries could prove beneficial in preventing structure disintegration due to H_2O and/or CO_2 attack from the surroundings, or may possibly act as flux pinning centres, even increasing the J_c. It also becomes important for considering the percolation limit which is different for conductivity measurements (at least 1/3 of HTSC to assure free conducting paths) and magnetic measurements (Maisnerr effect, at least 2/3 of HTSC to avoid penetration of magnetic field).

Not less important are the incongruent meltings taking place above approx. 1000°C. The 123 starting material transforms to a mixture of 211

and Y-deficient liquid when it is heated above its peritectic decomposition point. The 123 re-forms at the 211–liquid interface when the material is slowly cooled below the solidus, thereby encasing the 211 crystals inside 123. As is typical in any peritectic reaction, complete reaction between the high-temperature 211 solid and Cu-rich liquid is inhibited by the low-temperature 123 solid that is formed between them. This fractional solidification embeds some 211 crystals in the 123 matrix and segregates the Y-deficient liquid to the 123 grain boundaries. Cooling below the solidus transforms the liquid to a mixture of $BaCuO_2$ and CuO, see the upper DTA curve in Fig. 1. Homogeneous distribution of 211 in the melt can minimize the amount of fractional crystallization and thus increase the contact between 123 grains necessary for attaining the high J_c HTSCs. In turn, because 211 forms via a peritectic reaction between Y_2O_3 and Cu-rich melt, it can be reasoned that 211 could only be evenly distributed in the melt if Y_2O_3 was distributed in the melt equally well. It was found that the desired Y_2O_3 distribution could be created by heating the 123 starting material to approx. 1400°C and then splat-quenching. The repeated DTA runs can thus be seen to be the complex pattern of these peritectic reactions completed to various extents that are not helpful in the identification of individual steps.

The 123 melt directional processing based on fast quenching [23] and controlled reheating has already found practical applications in the preparation of bulk HTSC with high J_c values [24]. Also larger 123 crystals can be obtained by applying a temperature gradient across the crucible during very slow cooling of the solidified flux.

Another important factor is the low-temperature stability (< 820°C) of the 123 and/or 124 phases against decomposition [26] at very prolonged treatments (see the shaded area in Fig. 5, below).

TYPES OF FORMING PROCESSES AND THE OXIDATION STATE

In general we can distinguish several types of processes involved in the heterogeneous reactions taking place in the solid HTSC precursor:

(1) Internal reactions associated with the 123 phase formation and transition, such as (see Fig. 3) cation diffusion and ordering; *a–b* basal plane formation (nucleation of 123); oxygen intake and its ordering along the *b*-axis; possible exchange of both cation and anion positions; perovskite-layer multiplication or fault formation (metastable structures); and phase transformation (melting, etc.).

(2) Formation of interfacial and intergranular layers and their compositional and oxidation states, as well as their insulating properties.

(3) External reactions across the intergranular layers such as (see Fig. 2) transport of gases (O_2, CO_2); and transport of cations by diffusion and viscous flow.

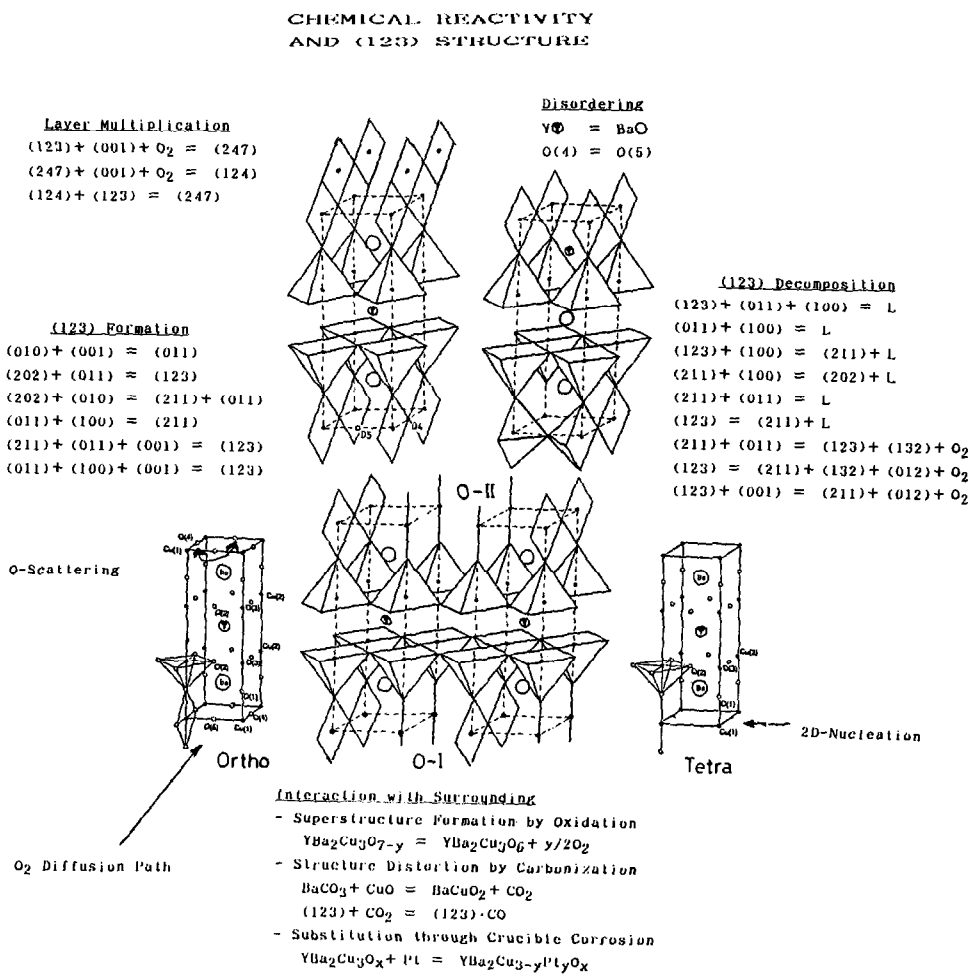

Fig. 3. Reactivity chart and possible superstructure networks.

Their mutual interaction is important but difficult to investigate. In particular, Hanic et al. [27] surprisingly indicated an increased reactivity at lower temperatures ($T < 340$°C) where two-dimensional (D_2) nucleation was found to best-fit their TG isothermal measurements of the oxygen intake. This could indicate that 2-D nucleation of a orthorhombic phase along the a–b basal face was the first to occur. At higher temperatures, ($T > 350$°C), however, an autocatalytic equation yields the best fit, probably indicating a kind of chemical ordering reaction, possibly associated with the oxygen redistribution (scattering) along the vacant (originally prohibited) O(5) voids. The frequently neglected effect of nucleation is found to be equally important in morphological studies of the initial stages of crystal growth from non-stoichiometric melts, see Fig. 2, upper-left corner, as

observed optically for the face build-up during the growth of HTSC single crystals [28]. The results of Stepanov et al. [29] are also of interest; they reported oxygen absorption in the 123 samples, using a high-pressure reactor with constant volume, in the temperature range 150–700°C with oxygen pressure from 1.4 to 10.7 atm. Two stages were described: the first is predictively related to the formation of a solid solution of oxygen in CuO(I) layers with $E = 0.7$ eV, resulting in the formation of more-or-less ordered –Cu–O– chains, while the second is associated with oxygen diffusion within the system of disordered chains $(Cu–O)_x$ with $E = 0.3$ eV. The growth of chains and their interaction to form the orthorhombic phase is said to be accompanied by a further decrease in reaction rate [29].

It is, however, difficult to find direct experimental evidence for the elementary processes taking place during oxygen intake. For example, the interface boundary of the 123 O ↔ T transformation was studied by direct observation in polarized light [30]. The diffusing oxygen forms orthorhombic domains with the ordered Cu(I)–O chains growing in the [1$\bar{1}$0] direction, their thickness being limited by elastic energy. After the critical thickness of the domains has been reached the chains start to grow in the perpendicular direction, thus forming the twin structure (see Fig. 2, bottom-left corner). Detailed study of the interface behaviour supports the concept of Khachaturyan and Morris [31] that there is neither a sharp nor a diffuse boundary between the O-I and O-II phases, and that the O ↔ T transition probably takes place via a series of stoichiometric compounds. Microdomains of the orthorhombic phase within the tetragonal matrix $(0.5 < x < 1)$ can be conveniently identified by TEM as the so-called tweed structure. When the oxygen content at a certain spot on the sample surface reaches a critical concentration, the domains of an O-II phase are formed, consequently growing to show coalescence and reorientation of the tweed structure [30]. Such nuclei, however, are formed at a low rate as demonstrated by the small number of twins packs observed [30]. A gradual increase of x then leads to an increase in the orthorhombic nature and transformation into an O-I phase, their crystallographic orientation being identical to that of the particular twin lamella [30].

Another complementary method is that of emanation thermal analysis (ETA) as reported earlier [32]. A more close inspection of the records, see Fig. 4, can indicate how the process of oxygen intake proceeds. Argon as a probe can penetrate only those paths that are free and big enough, i.e. along the vacant chains formed by O(5) voids. Occupation of oxygens increasing along the O(4) voids, can be stepwise as the ordered structures (superstructures) are gradually formed (see Fig. 3). As can be seen from Fig. 5 the precise stoichiometry of 123 is more complicated and closely related to the conditions of temperature, pressure and cooling-rate control. As shown above, it can be assumed that intermediate structures exist between the familiar fully oxygenated (ortho) and deoxygenated (tetra)

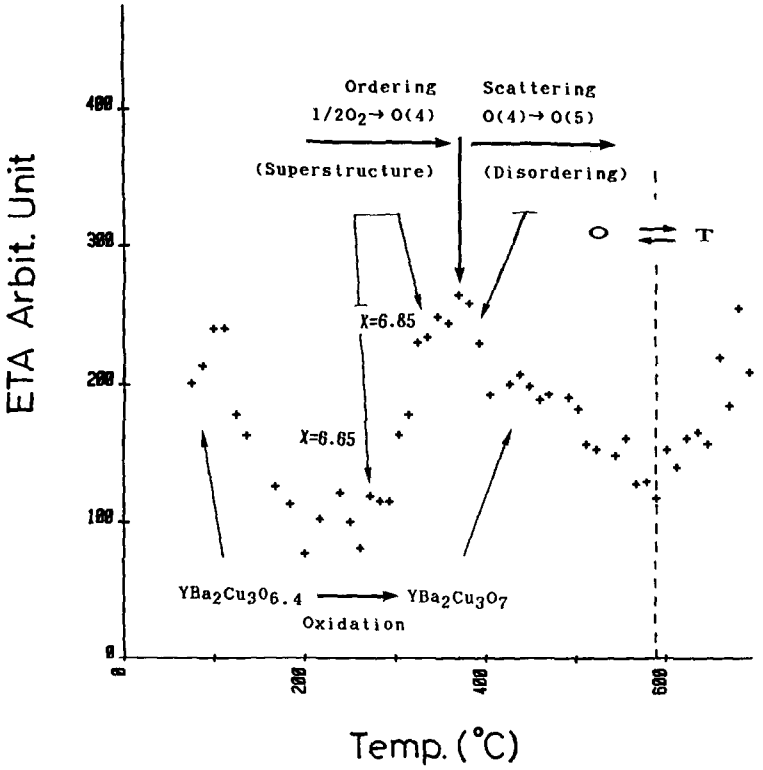

Fig. 4. ETA record at 1 K min^{-1} [32] (kindly provided by Prof. V. Balek of the Nuclear Research Institute, Řež).

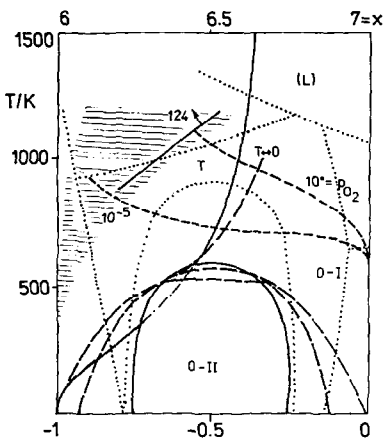

Fig. 5. Pseudo-binary phase diagram compiled on the basis of data published by Hauck et al. [56] (dotted lines), Khachaturyan et al. [57] (broken lines), Bayers and Ahn [36] (solid lines) and Voronin [58] (shaded area).

structures, i.e. the superlattice structures associated with $x = 6.65$ [2/5 0 0] and $x = 6.85$ [1/3 0 0] having full occupation every two in five or every second chain. Later on, owing to temperature scattering, oxygen also tends to occupy permanently some forbidden O(5) positions, essentially decreasing the diffusivity of argon through the lattice, see Fig. 4. The formation of these superlattices were confirmed by fine structure measurements [33] and calculation [34], and is in accordance with the published binary phase diagram of the oxygen dependence of the 123 structure, see Fig. 5, where the ortho-I and -II structures are separated by phase boundary lines, as in the deoxygenated tetragonal phase. The line of tetra–ortho-I transition terminates in a bicritical point, below which ortho-II is stable. The I–II ortho transition is found to be a second-order transition down to absolute zero, while the tetra–ortho-II transition is first order [34]. However, it is worth mentioning that the 123 phase is, in fact, unstable at normal conditions (T, P) and its region of stable existence should be marked by a special (dashed) area. The effect of oxygen is very important in the formation and stability of plausible phases inherent in the Y–Ba–Cu–O system, as shown in Fig. 6 [36–38].

Analogous to sample labelling by radioactive thorium acting as a source of argon which can be detected by means of ETA [32], another type of tracer measurements was made by Rothman et al. [39]. Polished samples of 123 ceramics were implanted with about 10^{17} atoms of ^{18}O using 5 keV ions to a depth of about 10^{-2} μm and annealed at 300–600°C; concentration profiles were then measured. A relatively high scatter in data was attributed to diffusion anisotropy; nevertheless, the reproducibility obtained was very good, giving a diffusion coefficient D of 9×10^{-6} exp(-0.89 eV/kT) cm^2 s^{-1}, i.e. an activation energy of about 86 kJ mol^{-1}. They compared their "tracer" D value with a more common "chemical" D, which is obtained by the standard technique of equilibrating a sample at one oxygen partial pressure and rapidly changing the pressure to another. The simultaneous measurement of a chosen property is then carried out as a function of oxygen stoichiometry, time and temperature. The discrepancy observed, i.e. $E = 1.7$ eV reported for isothermal resistivity measurements [40], and comparable values of $E = 1.5$–1.6 eV obtained by non-isothermal DSC measurements [41] of the heat evolved during the overall process of the oxygen absorption and its diffusion through the HTSC phase into grains of about 2 μm in size, was assumed to be a result of the sample dimensionality. The oxygen out-diffusion is assumed to be limited by a surface reaction due to the grain size and continuous porosity of the 123 ceramics.

Thorough investigations of the oxygen uptake and loss have been made by Ottavini et al. [42] and Tu et al. [43] using in situ resistivity measurements. Tu et al. [43] studied the out-diffusion by annealing the 123 ceramics in ambient helium at both constant heating rates (0.5–5°C min^{-1})

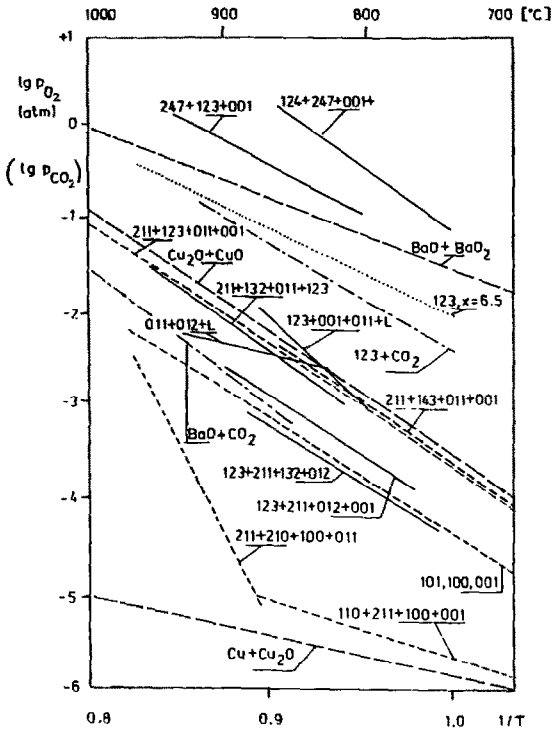

Fig. 6. Temperature dependence of oxygen pressure expressed for the various reactions in question drawn on the basis published by Bayers and Ahn [36] (dotted lines), Lindemer et al. [37] (solid lines), Borowiec and Kolbrecka [59] (broken lines) and Fjellvag et al. [60] (dot-dashed lines) and a survey of the phase diagrams by Šesták [38].

and temperatures (200–440°C) and found that it was independent of the stoichiometry x. Assuming the rate of oxygen loss is surface-reaction limited (R_1), they [43] determined a surface barrier of 1.7 eV. The study of the opposite process of in-diffusion was performed by annealing oxygen-deficient 123 ($x = 6.6$) in ambient oxygen; it was found to be strongly dependent on x with varying E (from 0.4 eV [42] and 0.5 eV [43] to 1.3 eV for $x = 7$) In the early stages of oxygen uptake, a near-surface layer of the 123 grains becomes saturated ($x = 7$), which then requires an activation energy of 1.3 eV for the oxygen atoms to diffuse through this fully oxidized shell and serves as a barrier, controlling the overall process of oxygen uptake. The oxygen diffusion is then understood as a non-conservative anisotropic process in which the empty O(1) lattice sites are either occupied or created. It is assumed [43] that in order for an O(1) oxygen atom to diffuse by exchanging with a vacancy, it must first move to a twinning position of an O(5) site. The activation energy for the twinning mechanism is therefore comparable with that of the vacancy mechanism, having the lowest change within the energy chart for the oxygen jumps available. The

superstructure, however, was not identified [42,43] although other fine resistivity measurements of well-annealed 123 samples indicated small plateaus [44,45] around the critical $x = 6.65$ and 6.85 values, which are not readily observable on the otherwise monotonous concentration dependence of critical temperature (T_c versus x).

The other interesting kinetic and mechanism considerations are associated with the crystallization of HTSC phases from quenched melts (glasses) [23,46,47], construction of the T–T–T diagrams [46,47], etc., which are mostly evaluated for more easily vitrifiable melts in the Bi–Ca–Sr–Cu–O system [24]. Of equal importance is a knowledge of the associated "average" phase diagrams [38] and of the thermodynamic stability of all possible phases [20].

KINETICS BY THERMAL ANALYSIS

Although thermoanalytical (TA) techniques are convenient methods for characterizing kinetically the reaction process and have been widely applied for the processes concerning superconductor formation and decomposition, it should be noted that the kinetic procedure has a phenomenological level of mathematical description for the macroscopically averaged experimental data [48]. The major problem in the kinetic study is the application of simple physico-geometrical models, valid for a single-step reaction, to the complicated consecutive reactions described above. Kaisersberger [49] analysed non-isothermal oxygenation processes in terms of consecutive reactions, and found that the oxygen intake is controlled by diffusion only up to $\alpha = 0.1$, whereas above this the TG curve is best fitted by an nth order chemical reaction. Superficially, the Kissinger method [50,51] for the kinetic analysis of DTA or DTG curves is likely to be suitable for evaluating the kinetic parameters, because in this method the value of E can be obtained without considering the kinetic model, $f(\alpha)$. (This has also been applied to the electrical resistivity measurements [43].) Figure 7 shows the TG and DTG curves for the oxygen loss and uptake processes in the 123 system. For the oxygen loss process in argon atmosphere, a change in the reaction mechanism is expected from the shape of the DTG curve. The three-dimensional diffusion, D_3, model was identified as the most appropriate model function within the range of fractional reaction, $\alpha < 0.6$. Mis-estimation of the $f(\alpha)$ leads to the distortion of the Arrhenius parameters [52], as is exemplified by the kinetic results for the oxygen loss process listed in Table 1. The E values of 120 and 172 kJ mol^{-1} determined by differential and integral methods are significantly different from that of 75 kJ mol^{-1}, reported by Nagase et al. [53], obtained for the process in high vacuum assuming the first-order reaction model.The wide temperature region applied for the kinetic calculation, which is beyond the implicit restriction for use of the integral method, explains the

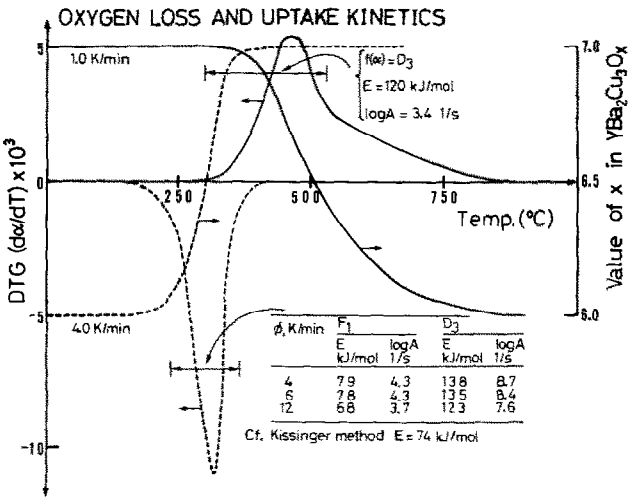

Fig. 7. TG and DTG curves for the oxygen loss (solid lines) and uptake (broken lines) processes in argon and oxygen atmospheres, respectively.

difference in the Arrhenius parameters determined by the respective methods. At the same time the differential method is sensitive for both the reaction process and experimental error. For the oxygen uptake process in oxygen atmosphere, the overall process can be well described by both the first order, F_1, and D_3 laws. These two laws give different values of E, approx. 70 and 130 kJ mol^{-1} respectively. The E value obtained assuming the F_1 law, 70 kJ mol^{-1}, corresponds to the values calculated by the Kissinger method, 71 kJ mol^{-1} [54]. The correspondence does not necessar-

TABLE 1

Arrhenius parameters calculated by assuming the possible kinetic model functions $f(\alpha)$ for the oxygen loss process of $YBa_2Cu_3O_x$ at the heating rate of 1.0 K min^{-1} in argon atmosphere ($0.1 \leq \alpha \leq 0.6$)

$f(\alpha)$	Achar, Brindley and Sharp method [61]			Coats and Redfern method [62]		
	E (kJ mol^{-1})	log A (s^{-1})	$-\gamma$ [a]	E (kJ mol^{-1})	log A (s^{-1})	$-\gamma$ [a]
D_1	89±4	2.0±0.3	0.9364	153±7	6.6±0.7	0.9909
D_2	104±4	2.8±0.3	0.9632	162±7	7.0±0.8	0.9940
D_3	120±4	3.4±0.3	0.9831	172±7	7.1±0.8	0.9967
D_4	109±4	2.6±0.3	0.9708	165±6	6.6±0.7	0.9949
R_2	22±3	−2.8±0.2	0.6957	78±4	1.2±0.2	0.9926
R_3	27±3	−2.0±0.2	0.7486	80±4	1.3±0.2	0.9943
F_1	38±2	−1.3±0.2	0.8845	99±4	1.6±0.2	0.9933

[a] Correlation coefficient of the linear regression analysis.

D, R and F indicate the standard kinetic laws [51] for diffusion, interface chemical reaction and first-order chemical reaction, respectively.

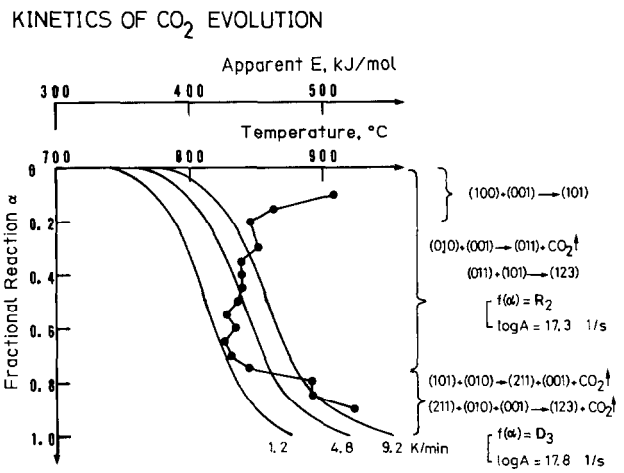

Fig. 8. TG curves for the CO_2 evolution process from the 123 feed mixture and the activation energies determined by the Ozawa method [55,63].

ily support the obedience to the F_1 law, because the Kissinger method is also derived on the basis of nth order reaction and the distortion in the E value by the use of an inappropriate model function is a mathematical consequence of this [52]. In this sense, the Arrhenius parameters obtained by TA methods can only be meaningful on the basis of a purely appropriate kinetics model function.

The kinetics of CO_2 evolution from $BaCO_3$ in the feed mixture is more complicated, as shown in Fig. 8. The value of E changes depending on the fractional reaction, α. The change probably arises owing to the change in the reaction pathway and the influence of processes which take place simultaneously with CO_2 evolution. The apparent values of E obtained for such a complicated process change drastically with the experimental conditions applied and do not always have physical significance. This is supported by the fact that the E value determined for the single (010) + (001) $\rightarrow$ (011) + CO_2 process, which seems to be the main reaction in the CO_2 evolution process from the 123 mixture [12], is the half of the value illustrated in Fig. 8 [55]. The careless application of kinetic study by thermal analysis [51] can disturb the comprehensive understanding of the kinetics and mechanisms of HTSC formation and decomposition.

CONCLUSIONS

Kinetic analysis based merely on phenomenological kinetic models cannot be conclusive in determining the complex reaction mechanism involved, not can TA data alone provide full understanding of the intermediate reaction steps. Nevertheless, diffusion is found to be the best fitted model

over major parts of TA curves which corresponds well with the assumed compositional reactions (changes such as oxygen and cation diffusion, the activation energies of which differ by about one order of magnitude) and structural (peritectic) reactions. The increased demands of high J_c materials have focused attention on grain morphology, shape and interfaces, stressing the need for complementary measurements that are well documented by the study of superstructure formation by microscopic and ETA investigations. The precise determination of the local grain boundary structure, state and chemistry thus remains a most important issue.

REFERENCES

1 A. Negishi, Y. Takahashi, R. Sakamoto, M. Kamimoto and T. Ozawa, Thermochim. Acta, 132 (1988) 50; 140 (1989) 41.
2 J. Šesták, T. Hanslik, M. Nevriva, E. Pollert and A. Triska, J. Therm. Anal., 33 (1988) 947.
3 G. Braun, G. Schuster, H. Ullmann, W. Matz and K. Henkel, Thermochim. Acta., 165 (1990) 261.
4 M. Kamimoto, Thermochim. Acta., 174 (1991) 153.
5 P.K. Gallagher, Adv. Ceram. Mater., 2 (1987) 632.
6 E.M. Vogal, G.W. Hull and J.-M. Tarascon, Mater. Lett., 6 (1988) 269.
7 P.K. Gallagher, Thermochim. Acta, 174 (1991) 85.
8 M. Nevriva, E. Pollert, J. Šesták and A. Triska, Thermochim. Acta, 127 (1988) 395.
9 D. Noel and L. Parent, Thermochim. Acta, 147 (1989) 109.
10 Le van Huan et al., Cryst. Res. Technol., 23 (1988) K125.
11 T. Ozawa, Thermochim. Acta, 133 (1988) 11.
12 A.M. Gadalla and T. Hegg, Thermochim. Acta, 145 (1989) 149.
13 E. Ruckenstein, S. Narain and N-L. Wu, J. Mater. Res., 4 (1989) 267.
14 E. Ruckenstein and N-L. Wu, Mater. Lett., 7 (1988) 165.
15 N-L. Wu, T-C. Wei, S-Y. Hou and S-Y. Wong, J. Mater. Res., 5 (1990) 2056.
16 C.J.R. Gonzales Oliver et al. Thermochim. Acta, 203 (1992) 353.
17 K.C. Goratta et al., J. Mater. Res., 5 (1990) 2760.
18 R. Decca, R. Isoardi and F. de la Cruz; lecture at the 6th Int. Workshop on Critical Currents, Cambridge, England, 1991.
19 P. Diko, K. Csach and J. Miskuf, J. Mater. Sci. Lett., 9 (1990) 386.
20 G.K. Moiseev, N.A. Vatolin, N.I. Ilyinych and J. Šesták, Thermochim. Acta, 198 (1992) 357.
21 D.R. Clark, T.M. Show and D. Dimes, J. Am. Ceram. Soc., 72 (1989) 1103.
22 Lijie Zhang et al., J. Am. Ceram. Soc., 72 (1989) 1997.
23 J. Šesták et al., Thermochim. Acta, 132 (1988) 35.
24 J. Šesták, in A. Narlikar (Ed.) Studies of HTSC, Nova Sci. Publ., Vol. 7, New York, 1991, p. 23.
25 M. Murakami et al. IEEE Trans. Mag., 27 (1991) 1497.
26 M. Fendorf, C.P. Burmester, L.T. Wille and R. Grousky, J. Less Comm. Met., 164/165 (1990) 84.
27 F. Hanic, I. Horvat and L. Galikova, Thermochim. Acta, 148 (1989) 229.
28 J. Scheel and P. Niedermann, J. Cryst. Growth, 94 (1989) 281.
29 A.A. Stepanov, N.G.Hainovsky, Y.T. Pavlyukhin and A.I. Rykov, Modern Phys. Lett., 4 (1990) 29.
30 N. Hudakova and P. Diko, Physica C, 167 (1990) 408.

31 A.G. Khachaturyan and J.W. Morris, Phys. Rev. Lett., 61 (1988) 215.
32 V. Balek and J. Šesták, Thermochim. Acta, 133 (1988) 23.
33 M. Herivieu et al., Mater. Lett., 8 (1989) 23.
34 D. de Fontaine, in J.L. Moran-Lopez and I.K. Schuller (Eds.), Oxygen Disorder Effect in HTSC, Plenum Press, New York, 1990, p. 75.
35 A. Barrera and D. de Fontaine, Phys. Rev. B, 39 (1989) 6727.
36 R. Bayers and B.T. Ahn, Ann. Rev. Mater. Sci., 21 (1991).
37 T.B. Lindemer et al., J. Am. Ceram. Soc., 73 (1990) 435.
38 J. Šesták, Pure Appl. Chem., 64 (1992) 125.
39 S.J. Rothman, J.C. Routbort, J.L. Nowicki and J.E. Baker, lecture at the DIMETA '88, Balantonfüred, Hungary, 1988.
40 K.N. Tu, S.I. Park and C.C. Tsuei, Appl. Phys. Lett., 51 (1987) 2158.
41 B.A. Glowacki, R.J. Higmore, K.F. Peters, L. Greer and J.E. Evetts, Supercond. Sci. Tech., 1 (188) 7.
42 G. Ottavini et al., Phys. Rev. B, 39 (1989) 9069.
43 K.N. Tu, N.C. Yeh, S.I. Park and C.C. Tsuei, Phys. Rev. B, 39 (1989) 304.
44 W.R. MicKinnon et al., Phys. Rev. B, 38 (1988) 73.
45 J.D. Jorgensen et al., Physica C, 153/155 (1988) 578.
46 J. Šesták, J. Therm. Anal., 36 (1990) 1639.
47 M. Tatsumisago et al., Appl. Phys. Lett., 54 (1989) 2268; 55 (1989) 600.
48 J. Šesták, J. Therm. Anal., 36 (1990) 1997.
49 E. Kaisersberger, lecture at 5th ESTAC, Nice, 1991.
50 H.E. Kissinger, Anal. Chem., 29 (1959) 1702.
51 J. Šesták, Thermophysical Properties of Solids, Elsevier, Amsterdam, 1984.
52 N. Koga, J. Šesták and J. Málek, Thermochim. Acta, 188 (1991) 333.
53 K. Nagase, H. Yokobayashi, M. Kikuchi, A. Tokiwa and Y. Syono, Thermochim. Acta, 175 (1991) 207.
54 C-L. Teske and H. Muller-Buschbaum, Z. Naturforsch., Teil A 43 (1988) 965.
55 N. Koga, unpublished result.
56 J. Hauck, K. Biekman and F. Zucht, Z. Phys. B, 67 (1987) 299.
57 A.G. Khachaturyan, S.V. Semenvskaja and J.W. Morris, Phys. Rev. B, 37 (988) 2243.
58 V.V. Voronin, Pure Appl. Chem., 64 (1992) 27.
59 K. Borowiec, K. Kolbrecka, J. Less Comm. Met., 163 (1990) 143.
60 H. Fjellvag et al., Acta Chem. Scand., A42 (1988) 178.
61 B.N. Achar, G.W. Brindley and J.H. Sharp, Proc. 1st Int. Clay Conf., Jerusalem, 1966, p. 67.
62 A.W. Coats and J.P. Redfern, Nature, 201 (1964) 68.
63 T. Ozawa, Bull. Chem. Soc. Jpn., 38 (1965) 1881.